POLITECNICO DI TORINO
Repository ISTITUZIONALE

A novel Finite Fracture Mechanics approach to assess the lifetime of notched components

Original
A novel Finite Fracture Mechanics approach to assess the lifetime of notched components / Mirzaei, A.M., Cornetti, P., Sapora, A.. - In: INTERNATIONAL JOURNAL OF FATIGUE. - ISSN 0142-1123. - 173:(2023), pp. 1-9. [10.1016/j.ijfatigue.2023.107659]

Availability:
This version is available at: 11583/2978245 since: 2023-04-29T15:45:48Z

Publisher:
Elsevier

Published
DOI:10.1016/j.ijfatigue.2023.107659

Terms of use:

This article is made available under terms and conditions as specified in the corresponding bibliographic description in the repository

Publisher copyright

(Article begins on next page)

04 November 2026

International Journal of Fatigue 173 (2023) 107659

Contents lists available at ScienceDirect

International Journal of Fatigue

journal homepage: www.elsevier.com/locate/ijfatigue

A novel Finite Fracture Mechanics approach to assess the lifetime of notched components

A.M. Mirzaei *, P. Cornetti, A. Sapora

Department of Structural, Geotechnical and Building Engineering, Politecnico di Torino, Corso Duca degli Abruzzi 24, 10129 Torino, Italy

ARTICLE INFO

Keywords:
Fatigue life
Lifetime estimation
Finite fracture mechanics
Notch
Fatigue strength

ABSTRACT

A novel model is proposed to assess the fatigue lifetime of notched components under uniaxial loading conditions in the medium/high-cycle fatigue regime. It is based on the Finite Fracture Mechanics approach, previously proposed in static and fatigue limit frameworks, according to which failure occurs when a stress and an energy condition are simultaneously satisfied. Basquin's equations are employed to catch the variation of input parameters based on SN data of a plain and a notched sample. The criterion is validated against various experimental data sets from the literature, encompassing different notch shapes, loading conditions and materials.

1. Introduction

Cracks, notches and holes are present in mechanical structures either for design purposes or due to wear and tear from usage and environmental conditions. Acting as stress raisers, they define the load-bearing capacity and operating time of the structural component. In this framework, fatigue failure i.e, the initiation and propagation of cracks in a material due to cyclic loading, represents undoubtedly the most common failure mechanism. Regarding deformations, the phenomenon can be categorized into low-cycle and high-cycle fatigue. The former is characterized by significant, repeated plastic deformation in each cycle, causing the material to undergo changes in its microstructure. In contrast, high-cycle fatigue typically involves lower stress amplitudes and is generally governed by elastic deformation, as the stress levels are below the yield stress. The arbitrary classification between high cycle and low cycle fatigue is typically based on the number of cycles and is often set around 10^3-10^4 cycles. It is worth to emphasize that the proposed model may not provide reasonable results for low cycle fatigue.

Focusing the attention on the linear elastic notch mechanics, the former studies addressing the failure behavior with an approach based on an structural length are those by Neuber [1] and Peterson [2]. They argued that the stress at a finite distance from the notch tip could be representative to assess the crack onset inside a structural element. However, it was only some decades later that the idea caught on through the formalism of the Theory of Critical Distances (TCD) by Taylor [3] and Susmel [4]. The linear-elastic TCD has proved to be highly accurate not only in predicting the fatigue limit, but also in estimating the fatigue lifetime of notched components failing in the medium-cycle fatigue regime [5], approximately between 10^4 to 10^6 cycles. Such an extension assumes that the critical distance decreases as the number of cycles increases by following a power law behavior. The two parameters describing the relationship depend on the material and loading ratio. Since both the critical distance and fatigue strength depend on the number of cycles, an iterative approach was proposed to get the number of cycles to failure. It is interesting to note that, in this framework, the TCD approach in the form of the line method has been found to be more accurate than the point method [6]. Due to its simplicity and robustness, the TCD has recently been developed to a variety of fatigue conditions, from torsional [7] to multiaxial [8,9] and variable amplitude loading [10–12]. The fatigue behavior of additively manufactured samples was also investigated [13–16].

A somehow similar approach is that proposed by Lazzarin and Zambardi in 2001 [17], and named averaged Strain Energy Density (SED) criterion. The basic idea is to compare the strain energy evaluated in a finite volume around the notch tip with a critical value that depends on the material properties; as the finite volume is determined by the material properties, this approach can also be considered a TCD model. The SED method was proposed to estimate the static and fatigue life of components weakened by sharp V-notches [17] and later extended to fatigue failure in different scenarios, like weldments [18], multiaxial loading conditions [19], and additively manufactured materials [20,21]. It is worth noting that TCD and SED predictions on the finite fatigue life of notched components were compared in [6] for several sets of experimental data. It was concluded that both approaches are capable of accurately predicting the lifetime of notched components, but TCD

* Corresponding author.
E-mail address: amir.mirzaei@polito.it (A.M. Mirzaei).

https://doi.org/10.1016/j.ijfatigue.2023.107659
Received 7 March 2023; Accepted 28 March 2023
Available online 31 March 2023
0142-1123/© 2023 The Authors. Published by Elsevier Ltd. This is an open access article under the CC BY license (http://creativecommons.org/licenses/by/4.0/).

Nomenclature

a	Length of a crack emanating from the notch root
a_k, b_k	Basquin's parameters for K_{If}
a_s, b_s	Basquin's parameters for σ_c
g_a	Geometrical function for the stress intensity factor (SIF) function
g_s	Geometrical function for the normal stress field
K_I	Mode I SIF
K_{Ic}	Plane strain fracture toughness
K_{If}	SIF at failure
l	Crack advancement for the FFM formulation in the fatigue life regime
l_f	Critical crack advancement for the FFM formulation in the fatigue life regime
l_S	Crack advancement for the FFM formulation in the static regime
l_R	Crack advancement for the FFM formulation in the fatigue limit regime
l_{TCD}	Critical distance for fatigue problems based on TCD
N	Number of cycles
N_f	Number of cycles to failure
R	Loading ratio
α	Notch opening angle
ΔK_{th}	Threshold value of the SIF range
$\Delta\sigma_0$	Plain fatigue limit
ρ	Notch radius
σ_a	Nominal (gross-section) stress amplitude
σ_c	Fatigue strength
σ_f	Failure stress
σ_u	Ultimate tensile stress
σ_y	Normal stress field

proved to be more robust for particular structural configurations, such as U-notches with low stress concentrations.

In the static framework, TCD and SED approaches are based on a length (the critical distance and the radius of the control volume, respectively), which is a material property. Actually, this can reveal detrimental for certain configurations, such small size devices, where this material length approaches (or even exceeds) the structural dimension. In order to overcome this drawback, Leguillon [22] and Cornetti et al. [23] introduced a coupled fracture criterion, usually referred to as Finite Fracture Mechanics (FFM). Similarly to TCD, FFM assumes that the crack extension occurs by finite amounts. Differently from TCD, the failure load and the critical distance are obtained by coupling two distinct requirements, a stress and an energy condition. Consequently, the finite crack extension becomes a structural parameter, i.e. it depends also on the geometry, differently from the TCD approach where the critical distance is just a material parameter. In the static framework, FFM was successfully exploited to assess the failure behavior of structures weakened by cracks, sharp or blunt V-notches, under mode I [24,25], mode II [26,27] or mixed mode loading conditions [28–31]. Later on, the approach was extended to fatigue scenarios encompassing - in the fatigue limit regime under uniaxial loadings - the crack-notch sensitivity [32], the effect of U- and sharp V-notches [33] (even under torsion [34]), welded T-joint fatigue behavior by considering residual stress [35], and the size effect of spheroidal voids and corrosion pits [36]. Recent comparisons between TCD and FFM estimations on the fatigue limit of V-notched components were performed by Shen et al. [37] and Liu et al. [38]. It was shown that the results by both criteria are similar, while FFM provides higher accuracy for blunter notches since the critical distance depends on the radius of curvature. Before proceeding, let us underline that several studies in the Literature [39,40] confirm that the critical distance is related to geometrical properties, thus supporting the hypotheses under which FFM was put forward.

In this paper, we present a fatigue failure criterion based on FFM to estimate the lifetime of notched components under constant amplitude uniaxial loading with given load ratio. The analysis is limited to the medium/high-cycle fatigue regime, under the assumption that stage II, where the crack growth is perpendicular to the loading direction, is the dominant stage during fatigue life. Therefore, the study will refer just to mode I loading conditions. The plastic zone size being negligible in the medium/high-cycle fatigue regime, a linear elastic mechanics will be exploited to determine the stress field and energy ahead of the notch tip. The FFM model is introduced in Section 2 and validated through available experimental data sets from the Literature in Section 3. Section 4 is voted to conclusions.

2. Finite Fracture Mechanics

In the static framework, FFM is a failure criterion based on a discrete crack extension, l_S, and on the simultaneous fulfilment of two conditions: a stress requirement and the energy balance [22,23]. Considering an arbitrary notched geometry (Fig. 1) under mode I loading, the FFM criterion (in its averaged version) reads:

$$\begin{cases} \dfrac{1}{l_S}\displaystyle\int_0^{l_S} \sigma_y(x)\,dx = \sigma_u \\ \dfrac{1}{l_S}\displaystyle\int_0^{l_S} K_I^2(a)\,da = K_{Ic}^2 \end{cases} \tag{1}$$

The first equation represents a stress condition, according to which failure occurs when the normal stress σ_y, averaged over a discrete crack length l_S, achieves the ultimate tensile stress σ_u. The second describes the energy balance: failure happens when the available energy release rate G for a crack extension l_S reaches the fracture energy G_c. This condition is rewritten in Eq. (1) in terms of the stress intensity factor (SIF) K_I and fracture toughness K_{Ic} by employing Irwin's relationship $K_I = \sqrt{(E\,G\,/(1-\nu^2))}$, where E is Young's modulus and ν is Poisson's ratio of the material. Equation (1) represents a system of two equations in two unknowns: the critical crack advance l_{Sf}, which is a structural parameter (since it depends on both the material and the geometry), and the failure stress σ_f, implicitly embedded in the $\sigma_y(x)$ and $K_I(a)$ functions. Note that, strictly speaking, the two equations in Eq. (1) should be two inequalities (with the left hand side larger than the corresponding right hand side) and the failure load is the minimum value fulfilling both them. However, for monotonically decreasing stress field $\sigma_y(x)$ and monotonically increasing SIF $K_I(a)$ (which is the the case considered herein), it can be easily checked that the minimum load is achieved when the two inequalities are strictly verified and, thus, Eq. (1) holds.

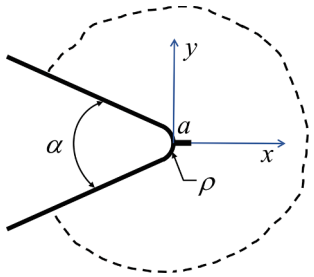


Fig. 1. Blunt V-notch geometry and Cartesian coordinate system located at the notch tip.

On the other hand, the extension of FFM to estimate the fatigue limit of notched elements can be formalized as follows [32,33]:

$$\begin{cases} \dfrac{1}{l_R}\displaystyle\int_0^{l_R} \Delta\sigma_y(x)\,dx = \Delta\sigma_0 \\ \dfrac{1}{l_R}\displaystyle\int_0^{l_R} \Delta K_I^2(a)\,da = \Delta K_{th}^2 \end{cases} \tag{2}$$

where $\Delta\sigma_0$ represents the fatigue limit or the high-cycle fatigue strength of the plain material, and ΔK_{th} denotes the threshold value of the SIF range for long crack propagation. It is worth noting that both material properties ($\Delta\sigma_0$ and ΔK_{th}) are referred to the same load ratio R, which characterises also the cyclic load applied to the considered notched component. Keeping the same physical meaning of its static counterpart, Eq. (2) represents again a system of two equations in two unknowns: the critical crack advance l_{Rf}, which interacts with the geometry under investigation, and the fatigue strength $\Delta\sigma_f$.

2.1. Fatigue lifetime estimation

As aforementioned, FFM can be employed to assess the failure behavior of notched components once the following material properties are provided: σ_u and K_{Ic} for the static case, Eq. (1); $\Delta\sigma_0$ and ΔK_{th} for the fatigue limit case, Eq. (2). In order to develop the FFM approach for fatigue life estimations, which lie in between the previous cases, a pair of material properties is now introduced, σ_c and K_{If}, representing the critical cycle stress and SIF amplitude, respectively. It is supposed that each of them depends on the number of cycles N by means of a power law relationship [4,41], namely:

$$\sigma_c = \sigma_c(N) = a_s\, N^{-b_s} \tag{3}$$

$$K_{If} = K_{If}(N) = a_k\, N^{-b_k} \tag{4}$$

where a_s, b_s and a_k, b_k are positive numbers, which reveal to be functions of material properties and loading conditions and can be derived by fitting experimental fatigue data (with 50% survival probability) generated from plain and cracked specimens, respectively, tested under uniaxial loading with the considered load ratio.

Equations (3) and (4) are also known as Basquin's equations [42]. The applicability of Eq. (3) is well-known. On the other hand, to justify Eq. (4), it can be argued that SN data for a cracked geometry approximately follow a line in the log–log plot, as illustrated in several studies [43–46]. Nevertheless, the process of machining sharp cracks proves to be challenging, in which the root radius always plays a role. A detailed discussion on the calibration of a_s, b_s (Eq. (3)) and a_k, b_k (Eq. (4)) will be provided in Section 2.2.

All in all, in order to assess the lifetime of notched components, FFM can be generalized as follows:

$$\begin{cases} \dfrac{1}{l}\displaystyle\int_0^{l} \sigma_y(x)\,dx = \sigma_c(N) \\ \dfrac{1}{l}\displaystyle\int_0^{l} K_I^2(a)\,da = K_{If}^2(N) \end{cases} \tag{5}$$

Once $\sigma_c(N)$ and $K_{If}(N)$ are known by means of Eqs. (3) and (4), Eq. (5) can be cast in the form:

$$\begin{cases} \dfrac{1}{l}\displaystyle\int_0^{l} \sigma_y(x)\,dx = a_s\, N^{-b_s} \\ \dfrac{1}{l}\displaystyle\int_0^{l} K_I^2(a)\,da = a_k^2\, N^{-2b_k} \end{cases} \tag{6}$$

Note that Basquin's equation holds true only in the middle number of cycles range, and thus limit cases are not covered by Eq. (6). However, the simplified form Eq. (6) allows us to proceed semi-analytically. In fact, assuming the normal stress and the SIF as the products of the nominal (gross-section) stress amplitude σ_a times a geometrical shape function, $\sigma_y(x) = \sigma_a\, g_s(x)$ and $K_I(a) = \sigma_a\, g_k(a)$, Eq. (6) can be definitively rewritten as:

$$\begin{cases} N = l^{1/b_s}\left[\dfrac{\sigma_a}{a_s}\displaystyle\int_0^{l} g_s(x)\,dx\right]^{-1/b_s} \\ N = \sqrt{l^{1/b_k}\left[\left(\dfrac{\sigma_a}{a_k}\right)^2\displaystyle\int_0^{l} g_k^2(a)\,da\right]^{-1/b_k}} \end{cases} \tag{7}$$

According to Eq. (7), the two FFM unknowns are now represented by the number of cycles to failure N_f, and the critical crack advancement l_f. In the proposed approach, it is important to note that N_f corresponds to the number of cycles at which a crack with a length of l_f would appear. For a fixed material and loading ratio, by equaling the right-hand sides of both equations, and solving the implicit equation in l, the critical length l_f can be achieved for different stress amplitudes σ_a. The value of l_f must be then substituted into one of the two equations in (7) to get the number of cycles to failure, N_f.

Note that the coupled FFM approach can also be presented considering a "pointwise" stress criterion [22] instead of an averaged one:

$$\begin{cases} \sigma_y(x = l) = \sigma_c(N) \\ \dfrac{1}{l}\displaystyle\int_0^{l} K_I^2(a)\,da = K_{If}^2(N) \end{cases} \tag{8}$$

Analytical manipulations similar to the previous one lead to:

$$\begin{cases} N = \left[\dfrac{\sigma_a}{a_s}\, g_s(l)\right]^{-1/b_s} \\ N = \sqrt{l^{1/b_k}\left[\left(\dfrac{\sigma_a}{a_k}\right)^2\displaystyle\int_0^{l} g_k^2(a)\,da\right]^{-1/b_k}} \end{cases} \tag{9}$$

which can be solved analogously to Eq. (7). Note that the term *pointwise* is not rigorous since it is required $\sigma_a > \sigma_c$ over the whole length l. However, since the stress field is monotonically decreasing, this condition is consistent with the first equation in Eq. (8).

2.2. Calibration of a_s, b_s and a_k, b_k

In order to estimate a_s and b_s a best fitting interpolation procedure can be applied to the experimental data related to plain samples, thus referring to classical Wohler's curves. Related tests are commonly carried out for different material and loading ratios/conditions, following specific standard codes. The calibration procedure must refer to the medium/high cycle regime, since the failure behavior is generally different in the low cycle regime. As already outlined, depending on the material, the linear elastic assumption could be inaccurate for $N < 10^3$-10^4 and using stress-based approaches over this range can lead to considerable error in calculations. Although two SN data are sufficient to calibrate a_s and b_s, due to the typically high scatter of fatigue experimental data, it is recommended to employ more data (covering the whole range of interest) to increase the accuracy of the estimation. In Section 3 this task will be accomplished by means of an interpolation procedure based on linear least squares in the log–log plane.

On the other hand, in order to estimate a_k and b_k one can refer to experiments related to a sharp cracked geometry, or to a sufficiently sharp V-notched one, taking into account that Williams' eigenvalues are approximately constant over the amplitude range $0° \le \alpha \le 90°$ [47]. If either experimental results on sharp cracks or V- notches are not available or the presence of the root radius is not negligible (as it happens for most notched configurations), a second approach can be proposed. It employs an inverse calibration of Basquin's equation (Eq. (4)) by considering experimental data (in the medium–high cycle regime) related to a notched sample. Note that if data related to different

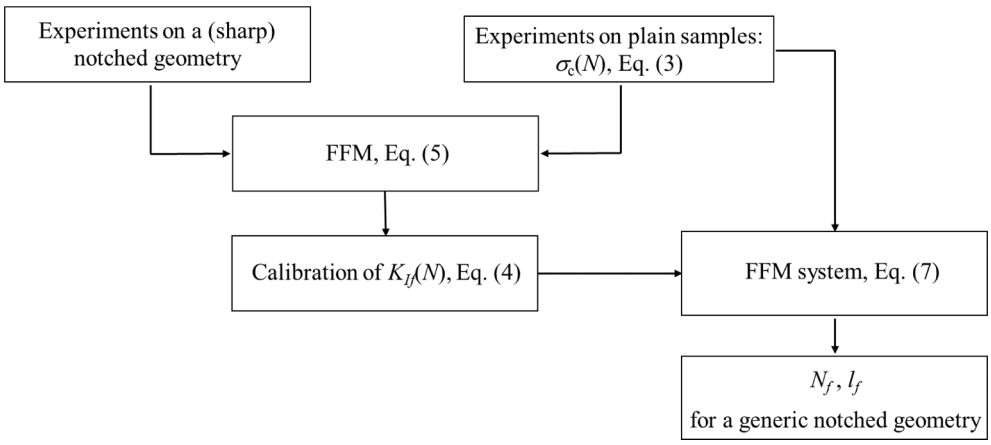


Fig. 2. Flowchart representing the procedure to employ the FFM model for a given material and loading ratio.

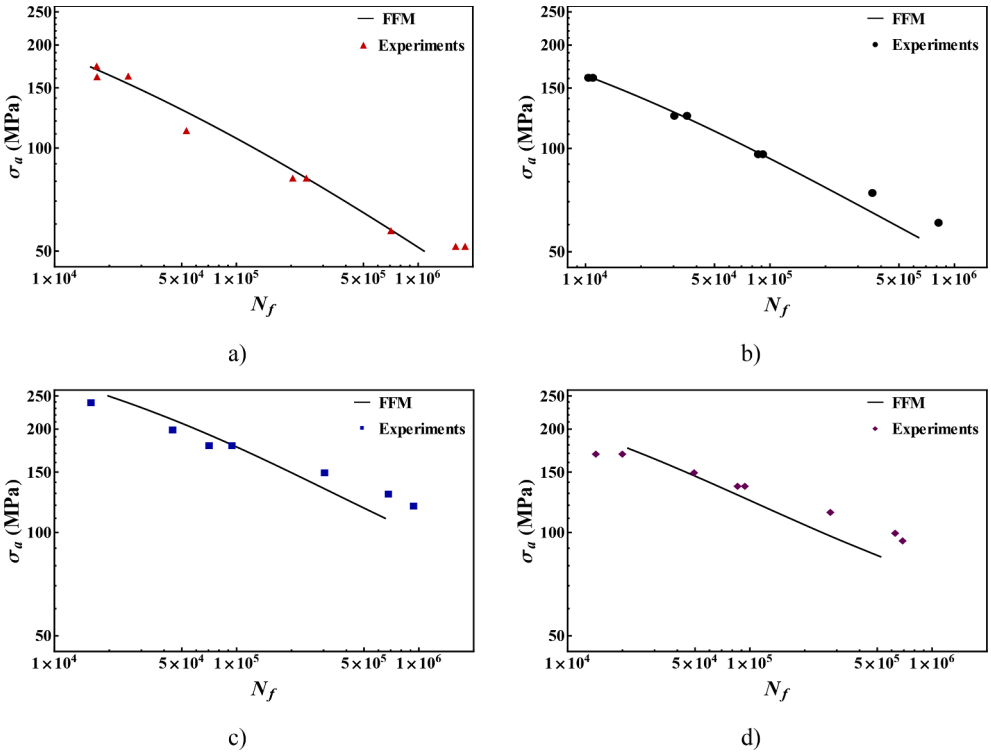


Fig. 3. Nominal (gross-section) stress amplitude vs. number of cycles to failure for different notched samples made of EN3B steel ($R = -1$), a) V-notch, b) U-notch, c) Hole $\rho = 1.75$ mm, d) Hole $\rho = 4$ mm. Solid black lines refer to the predictions by average FFM formulation (Eq. (7)) and the experimental data from [5] are shown by markers.

configurations are available, it is advisable to utilize the sharpest geometry to calibrate a_k and b_k, coherently with previous observations and studies [5,41,48]. More in detail, once the applied stress and the number of cycles to failure are known experimentally, from the first equation of the system (5), l_f is recovered; then, the second equation provides K_{If}. Repeating the procedure for different stress amplitudes (it is again recommended to employ more data covering the whole range of interest) allows one to get $K_{If} = K_{If}(N)$ and thus the calibration of a_k and b_k through a simple interpolation procedure based on linear least squares.

In summary, the flowchart in Fig. 2 shows the steps to employ for FFM estimation on the fatigue life of notched components.

3. FFM validation

In this section, the FFM model presented in Section 2 is validated against experimental data referring to different notch shapes and sizes, loading conditions, and materials [5,13,49]. In order to evaluate the shape function $g_s(x)$ related to the normal stress $\sigma_y = \sigma_y(x)$ for all geometries, the asymptotic stress approach proposed by Mirzaei et al. [50] is employed. The proposed solution allows to obtain the stress field around different notch shapes over short to long distances, by considering the effect of higher order terms [51]. On the other hand, FE analyses are carried out for each geometry through Abaqus® software to

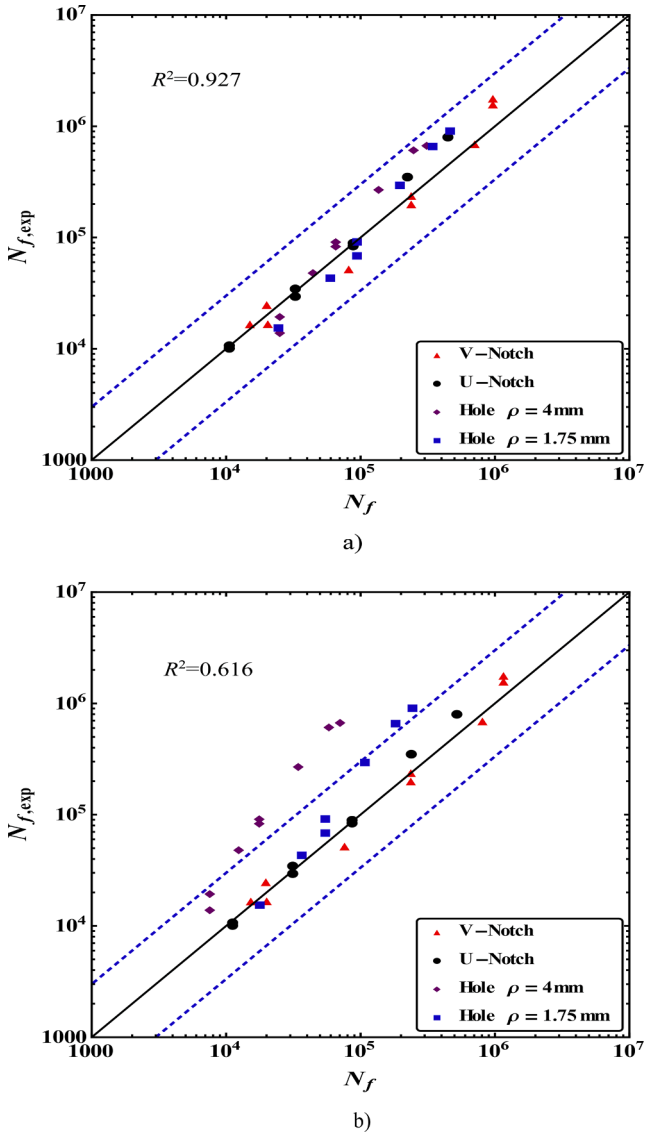


Fig. 4. Number of cycles to failure for different notched samples made of EN3B steel ($R = -1$): experimental data [5] vs. FFM predictions according to the average a) and the pointwise b) formulations. The dashed lines represent 1/3 and 3 scatter bands.

determine the shape function $g_k(a)$ related to $K_I = K_I(a)$, for a wide range of a. Samples are meshed by 8-node biquadratic elements, and convergence analysis is conducted to ensure the independence of numerical results from the mesh size.

3.1. Different notch shapes

Let us start the validation of the FFM model by employing the experimental results presented in [5] and referring to single edge notched plates made of EN3B steel, plain or weakened by different notch shapes: a V-notch with an opening angle $\alpha = 60°$ and notch tip radius $\rho = 0.12$ mm; a U-notch ($\alpha = 0°$) with $\rho = 1.5$ mm; a central circular hole with two different radii, $\rho = 1.75$ and 4 mm. Tests were performed under tension–compression loading (loading ratio $R = -1$), and the number of cycles to failure N_f was determined by 50% decrease in initial stiffness. More details can be found in [5]. Using a best fitting procedure on experimental data for the plain specimens, we got $\sigma_c = 935\, N^{-0.107}$ MPa, Eq. (3). On the other hand, considering all data related to the V-notch

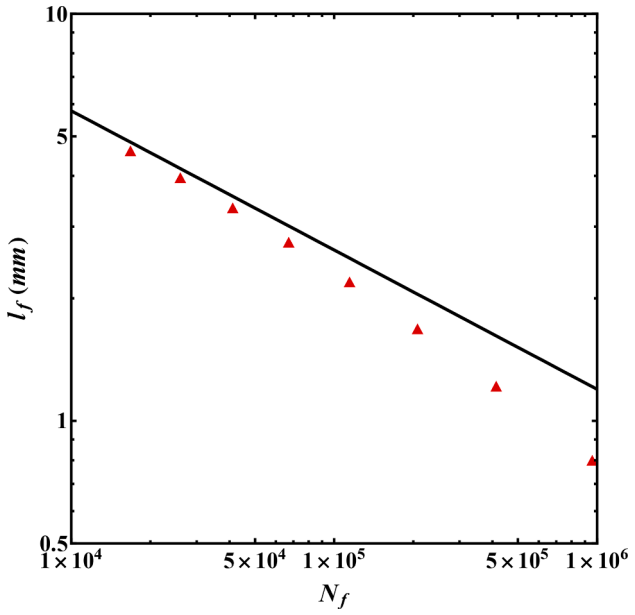


Fig. 5. Crack advancement (critical distance) l_f as a function of number of cycles for the V-notched geometry [5]: FFM (symbols) and TCD (solid line) estimations.

geometry (which is the sharpest one) to calibrate a_k and b_k in Eq. (4), yields $K_{If} = 1530\, N^{-0.381}$ MPa$\sqrt{\text{m}}$ for the average FFM formulation (Eq. (5)), plus $K_{If,p} = 504\, N^{-0.300}$ MPa$\sqrt{\text{m}}$ for the pointwise one (Eq. (8)). In Fig. 3, the amplitude of the nominal (gross-section) stress and its corresponding number of cycles to failure (SN diagram) for each notched geometry are plotted along with predictions of average FFM formulation (Eq. (7)).

For this set of experimental data, the model performance is quite good for V- and U-notches. However, when applied to holes, it is slightly unconservative for lower cycles, then conservative for higher cycles. To have a more thorough assessment of the proposed model, Fig. 4a shows the fatigue life predictions using FFM average version (Eq. (7)) vs. its corresponding experimental data, and Fig. 4b is related to the pointwise version (Eq. (9)). In Fig. 4 the horizontal axis shows the estimated life,

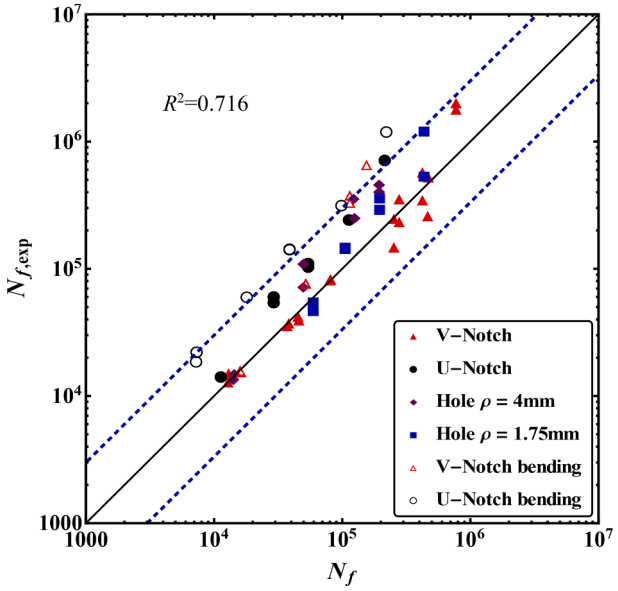


Fig. 6. Number of cycles to failure for different notched samples made of EN3B steel ($R = 0.1$): experimental data [5] vs. FFM predictions. The dashed lines represent 1/3 and 3 scatter bands.

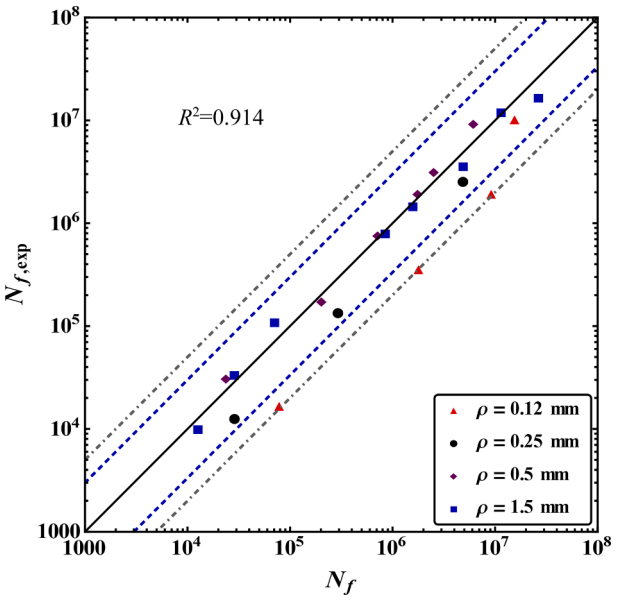


Fig. 7. Number of cycles to failure for samples weakened by a circular hole: experimental data on Al 2024-T351 ($R = -1$) [49] vs. FFM predictions. The dashed blue lines represent the scatter bands of 1/3 and 3, whereas the dotted-dashed gray lines illustrate the scatter bands of 1/5 and 5. (For interpretation of the references to colour in this figure legend, the reader is referred to the web version of this article.)

and the vertical axis illustrates the experimental number of cycles to failure. Therefore, the region above the solid black line refers to conservative predictions.

From Fig. 4, it can be argued that FFM predictions of fatigue life for different geometries are promising, considering the range of data from 10^4 to 10^6 cycles. All average stress FFM predictions from Eq. (7) are comprised in the scatter band 1/3 and 3; the results by the pointwise FFM formulation, Eq. (9), are less accurate, even if on the conservative side. In order to have a check on model performances, *R*-squared error (R^2 or the coefficient of determination) is employed referring to the natural logarithm transformation of the data. In this case, for FFM-average, it is equal to 0.702 and to 0.649 for FFM-pointwise. Accordingly, we will present the estimations only by the first (i.e., average stress) FFM approach (Eq. (5)) onwards.

Finally, in order to further discuss FFM parameters, the crack advancement l_f is presented for the V-notched geometry in Fig. 5. Approximating l_f by linear regression yields $l_f = 245\ N^{-0.406}$.

In this figure, the TCD critical distance, $l_{TCD} = 2 \times 67.4\ N^{-0.342}$ (see Eq. (17) in [5]), is also reported. As expected, the crack advancements for both methods are similar, particularly for lower cycle regimes. It is worthwhile to emphasize once more that l_{TCD} is assumed to vary according to a power law equation on *N*, thus representing an input to the model. On the contrary, l_f becomes an output of the system in Eq. (8) according to the proposed FFM approach.

3.2. Different uniaxial loading conditions

In order to demonstrate the applicability of the FFM model in fatigue life estimation for different notch shapes under different uniaxial loading conditions, another set of experimental data related to EN3B steel and reported in [5] is taken into account. It refers to six notched geometries tested under tension–tension ($R = 0.1$), under either tensile

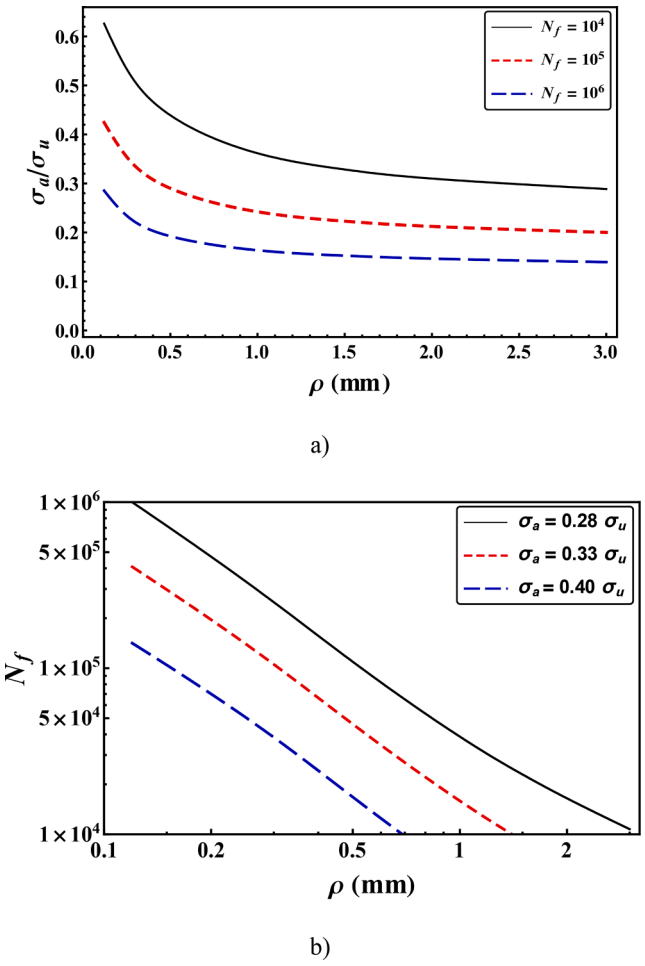


Fig. 8. a) effect of the hole radius on nominal (gross-section) stress amplitude for constant fatigue life. b) effect of the hole radius on the fatigue life under constant applied stress in a log–log plot. Results refer to Al 2024-T351 samples [49] geometry under tension–compression loading conditions ($R = 1$).

or bending loading conditions. The tensile samples have the same geometry as those reported in Section 3.1. The bending specimens (which are about 4 times thicker than tensile ones) consist of an edge V-notched plate with an opening angle $\alpha = 45°$ and radius $\rho = 0.383$ mm, and an edge U-notched ($\alpha = 0°$) plate with $\rho = 5$ mm.

For this data set, we obtain $\sigma_c = 1920\ N^{-0.178}$ MPa (Eq. (3)), and $K_{If} = 436\ N^{-0.312}$ MPa$\sqrt{m}$ by calibrating a_k and b_k using the tensile V-notched geometry (i.e., the sharpest one, Eq. (4)).

From Fig. 6, it can be seen that the predictions of the proposed model are in good agreement with the experimental results. Basically, they reveal more conservative for the bending samples. This can be explained in light of the fact that SN data related to the plain specimens differ from tensile to bending loading conditions [52,53]: for the range of cycles considered between 10^4 and 10^6, plain specimens under bending have a longer fatigue life, ranging from 18 to 10 percent, respectively [5]. Hence, more accurate results can be obtained by calculating the strength variation (i.e., calibrating a_s and b_s) on the data related to the bending loading conditions. Furthermore, the considerable difference -more than four times- in terms of thickness may contribute to the lower accuracy since 3D effects are ignored [54–56].

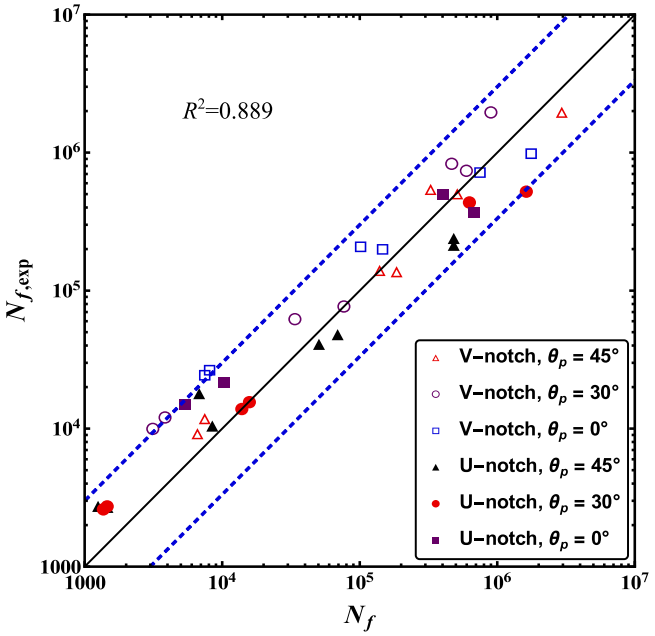


Fig. 9. Number of cycles to failure for different notch geometries and manufacturing angles, PLA ($R = 0$): experimental data [13] vs. FFM predictions. The dashed lines represent 1/3 and 3 scatter bands.

3.3. Failure size effect

The failure size effect in solid mechanics has drawn scientific attention for years, as it plays a major role in the engineering design of small to big structures. To check the ability of FFM to catch the phenomenon in fatigue life predictions, the data related to a plate weakened by circular holes having different radii ($\rho = 0.12$, 0.25, 0.5, 1.5 mm) is considered [49]. Because the fatigue lives range from 10^4 to 10^8, this is an intriguing set of experiments to demonstrate the model's applicability after calibration over a wide range of cycles. The involved material was a high-strength aluminum called Al 2024-T351, and tests were run under tension–compression loading conditions ($R = -1$). In this case, after determining $\sigma_c = 1380\, N^{-0.146}$ MPa (Eq. (3)), and employing all the data related to the hole with $\rho = 1.5$ mm for the calibration procedure, $K_{If} = 64.7\, N^{-0.205}$ MPa$\sqrt{\text{m}}$ is estimated. On the other hand, choosing the smallest hole (which is also admissible in absence of a sharp geometry) as the reference would lead to $K_{If} = 26.6\, N^{-0.170}$ MPa$\sqrt{\text{m}}$, affecting slightly the related predictions.

It can be argued that FFM results are in reasonably good agreement with experimental data, Fig. 7. The model provides predictions within the scatter bands of 1/3 and 3 life factors for $\rho = 0.5$ and 0.25 mm (which are 3 and 6 times smaller). On the other hand, considering the smallest hole with $\rho = 0.12$ mm (12.5 times smaller than $\rho = 1.5$ mm), fatigue life estimations fall in 1/5 and 5 life scatter bands. It is worthwhile noting that some studies in the Literature predicted this set of experimental data with higher accuracy [39,40], but they required the calibration of additional parameters, revealing thus more complex.

In Fig. 8, a parametric study is performed to show the effect of hole radius on the lifetime of notched components. Considering Fig. 8a, it can be seen that by increasing the fatigue life, the effect of the notch radius decreases. Fig. 8b shows that the notch effect is higher for lower applied stress (high cycle fatigue). Both figures illustrate that the smaller hole radius, the higher its effect on fatigue life i.e., the higher the number of cycles to failure.

3.4. Additively manufactured samples

In order to further validate the model, a non-metallic material is now considered, polylactide (PLA) [13]. Specimens were double edge notched - a V-notch with $\alpha = 35°$, $\rho = 0.383$ mm and a U-notch with $\rho = 1$ mm - with width and net width of 12.5 and 3 mm, respectively, and were tested under zero-tension loading conditions ($R = 0$). The samples were fabricated using Fused Deposition Modeling technology in their as-built condition. Three different manufacturing angles were taken into consideration: $\theta_p = 0°$, 30°, and 45°, where θ_p represents the angle between the longitudinal axis of the sample and the principal direction of manufacturing. Related stress vs. strain curves proved the validity of using a linear-elastic model [11]. Besides, the material behavior is assumed to be homogeneous and isotropic, coherently with the analysis carried out by Ezeh and Susmel [57]. Indeed, the Authors performed a large number of experimental tests on PLA, arguing that the effect of the filament's orientation on fatigue performances could be ignored. Considering plain specimen, it is determined $\sigma_c = 47.8\, N^{-0.161}$ MPa,

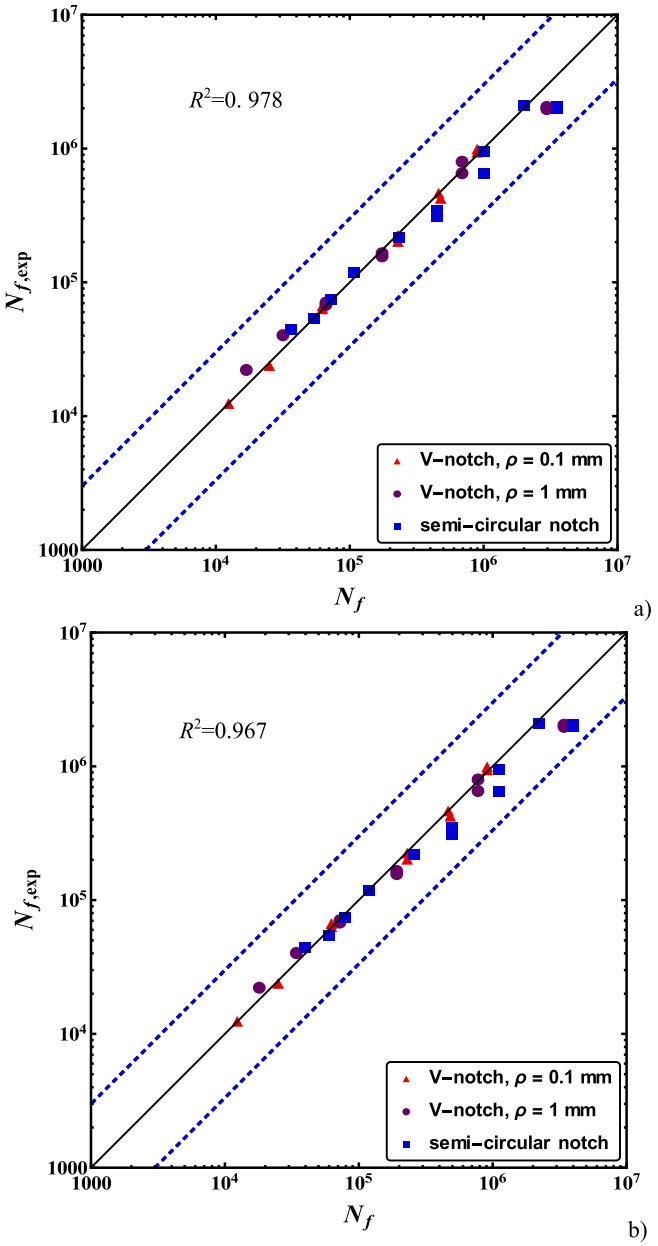


Fig. 10. Number of cycles to failure for different notched samples made of Inconel 718 ($R = 0$) [58]: experimental data vs. a) FFM, b) TCD predictions. The dashed lines represent the scatter bands of 1/3 and 3.

whereas employing the data related to the sharpest notch to calibrate a_k and b_k result in $K_{If} = 25.9\ N^{-0.195}$ MPa$\sqrt{\text{m}}$.

Despite the simplified assumptions, it can be seen that the FFM is able to estimate the fatigue lives of additively manufactured specimens with different manufacturing angles within the band of 1/3 and 3 life factors (Fig. 9). On the other hand, this set of experiments illustrates one important peculiarity of FFM: the crack advancement is not only a material constant but also a geometrical property. As a matter of fact, TCD approach in the form of the line method cannot be applicable in this case, because the critical distance exceeds the net width of the geometry [13]. This behavior already emerged in the static failure regime, both for plain and cracked elements [23,36].

Finally, another set of experimental data related to additively manufactured materials is taken into account [58]. It refers to Inconel 718: double edge notched specimens were machined using selective laser melting with manufacturing angle $\theta_p = 0°$ and tested under zero-tension loading conditions ($R = 0$). The notched geometries consisted of a V-notch $\alpha = 90°$, with two different radii $\rho = 0.1$ and 1 mm, plus a semi-circular notch with $\rho = 5$ mm.

Coherently with what done before, we assume again that the material behavior is homogeneous and isotropic. According to the results from the plain geometry and the sharpest V-notched ($\rho = 0.1$ mm) one, the following critical parameters are obtained: $\sigma_c = 13000\ N^{-0.272}$ MPa and $K_{If} = 555\ N^{-0.319}$ MPa$\sqrt{\text{m}}$. Fig. 10a shows a very fine correlation between FFM predictions by Eq. (7) and experimental data, all these lying in between scatter bands. For this data set, TCD is also employed in the version of line method [5]: related results are reported in Fig. 10b. Comparing Figs. 10a and 10b, we can argue that, for this set of experimental data, FFM predictions are slightly better than TCD's one.

4. Conclusions

From the present investigation, conclusions can be itemized as follows:

1. A novel criterion for finite life estimation of notched components under uniaxial cycling loading was proposed by extending the coupled FFM approach to fatigue.
2. Basquin's equations are used to calibrate the strength and SIF at failure by employing SN data of a plain and a (sharp) notched geometry, respectively. After calculating the proper geometrical shape functions for the stress field and SIF, the FFM approach predicts the lifetime of any notched geometry under different loading amplitudes, given the material and loading ratio.
3. Comparison with experimental data sets related to different notched structural configurations proved the soundness of the model.
4. The effect of the notch radius and applied stress on the fatigue lifetime of a circularly holed plate was assessed. Results revealed that FFM is able to predict successfully the size effect of notched components over a wide range of lives.
5. The FFM crack advancement is a function of both the material and the geometry (beyond the loading ratio and the number of cycles to failure). This means that FFM can be employed for structures where the TCD critical distance approaches or exceeds the net width of the specimen, being thus inapplicable or unreliable.
6. Further developments of the FFM model in the framework of lifetime of notched components include the case of variable amplitude loading, multiaxial loading, and three-dimensional effects.

Declaration of Competing Interest

The authors declare that they have no known competing financial interests or personal relationships that could have appeared to influence the work reported in this paper.

Data availability

Data will be made available on request.

Acknowledgements

The authors acknowledge the funding from the European Union's Horizon 2020 research and innovation program under the Marie Skłodowska-Curie grant agreement No 861061 – NEWFRAC Project.

References

[1] Neuber H. Theory of notch stresses: principles for exact calculation of strength with reference to structural form and material. 1961:293p.
[2] Peterson RE. Notch sensitivity. Met Fatigue 1959:293–306.
[3] Taylor D. Geometrical effects in fatigue: a unifying theoretical model. Int J Fatigue 1999;21:413–20. https://doi.org/10.1016/S0142-1123(99)00007-9.
[4] Susmel L. Multiaxial notch fatigue. Oxford: Woodhead Publishing: Elsevier; 2009.
[5] Susmel L, Taylor D. A novel formulation of the theory of critical distances to estimate lifetime of notched components in the medium-cycle fatigue regime. Fatigue Fract Eng Mater Struct 2007;30:567–81.
[6] Hu Z, Berto F, Hong Y, Susmel L. Comparison of TCD and SED methods in fatigue lifetime assessment. Int J Fatigue 2019;123:105–34. https://doi.org/10.1016/j.ijfatigue.2019.02.009.
[7] Susmel L, Taylor D. The Theory of Critical Distances to estimate finite lifetime of notched components subjected to constant and variable amplitude torsional loading. Eng Fract Mech 2013;98:64–79. https://doi.org/10.1016/j.engfracmech.2012.12.007.
[8] Susmel L, Taylor D. The Modified Wöhler Curve Method applied along with the Theory of Critical Distances to estimate finite life of notched components subjected to complex multiaxial loading paths. Fatigue Fract Eng Mater Struct 2008;31:1047–64. https://doi.org/10.1111/j.1460-2695.2008.01296.x.
[9] Branco R, Costa JD, Borrego LP, Berto F, Razavi SMJ, Macek W. Comparison of different one-parameter damage laws and local stress-strain approaches in multiaxial fatigue life assessment of notched components. Int J Fatigue 2021;151:106405. https://doi.org/10.1016/j.ijfatigue.2021.106405.
[10] Susmel L, Taylor D. The Theory of Critical Distances to estimate lifetime of notched components subjected to variable amplitude uniaxial fatigue loading. Int J Fatigue 2011;33:900–11. https://doi.org/10.1016/j.ijfatigue.2011.01.012.
[11] Susmel L, Taylor D. Estimating lifetime of notched components subjected to variable amplitude fatigue loading according to the elastoplastic theory of critical distances. J Eng Mater Technol 2015;137. https://doi.org/10.1115/1.4028927.
[12] Susmel L, Taylor D. A critical distance/plane method to estimate finite life of notched components under variable amplitude uniaxial/multiaxial fatigue loading. Int J Fatigue 2012;38:7–24. https://doi.org/10.1016/j.ijfatigue.2011.11.015.
[13] Ezeh OH, Susmel L. On the notch fatigue strength of additively manufactured polylactide (PLA). Int J Fatigue 2020;136:105583. https://doi.org/10.1016/j.ijfatigue.2020.105583.
[14] Molaei R, Fatemi A. Fatigue performance of additive manufactured metals under variable amplitude service loading conditions including multiaxial stresses and notch effects: experiments and modelling. Int J Fatigue 2021;145:106002. https://doi.org/10.1016/j.ijfatigue.2020.106002.
[15] Benedetti M, Santus C. Notch fatigue and crack growth resistance of Ti-6Al-4V ELI additively manufactured via selective laser melting: a critical distance approach to defect sensitivity. Int J Fatigue 2019;121:281–92. https://doi.org/10.1016/j.ijfatigue.2018.12.020.
[16] Molaei R, Fatemi A, Phan N. Notched fatigue of additive manufactured metals under axial and multiaxial loadings, part II: Data correlations and life estimations. Int J Fatigue 2022;156:106648. https://doi.org/10.1016/j.ijfatigue.2021.106648.
[17] Lazzarin P, Zambardi R. A finite-volume-energy based approach to predict the static and fatigue behavior of components with sharp V-shaped notches. Int J Fract 2001;112:275–98. https://doi.org/10.1023/A:1013595930617.
[18] Berto F, Campagnolo A, Chebat F, Cincera M, Santini M. Fatigue strength of steel rollers with failure occurring at the weld root based on the local strain energy values: modelling and fatigue assessment. Int J Fatigue 2016;82:643–57. https://doi.org/10.1016/j.ijfatigue.2015.09.023.
[19] Berto F, Campagnolo A, Lazzarin P. Fatigue strength of severely notched specimens made of Ti–6Al–4V under multiaxial loading. Fatigue Fract Eng Mater Struct 2015;38:503–17. https://doi.org/10.1111/ffe.12272.
[20] Razavi SMJ, Ferro P, Berto F, Torgersen J. Fatigue strength of blunt V-notched specimens produced by selective laser melting of Ti-6Al-4V. Theor Appl Fract Mech 2018;97:376–84. https://doi.org/10.1016/j.tafmec.2017.06.021.
[21] Razavi SMJ, Askes H, Berto F, Susmel L. Length scale parameters to estimate fatigue lifetime of 3D-printed titanium alloy Ti6Al4V containing notches in the as-manufactured condition. Int J Fatigue 2022:107348. doi: 10.1016/j.ijfatigue.2022.107348.
[22] Leguillon D. Strength or toughness? A criterion for crack onset at a notch. Eur J Mech 2002;21:61–72.
[23] Cornetti P, Pugno N, Carpinteri A, Taylor D. Finite fracture mechanics: a coupled stress and energy failure criterion. Eng Fract Mech 2006;73:2021–33. https://doi.org/10.1016/j.engfracmech.2006.03.010.

[24] Carpinteri A, Cornetti P, Pugno N, Sapora A, Taylor D. A finite fracture mechanics approach to structures with sharp V-notches. Eng Fract Mech 2008;75:1736–52. https://doi.org/10.1016/j.engfracmech.2007.04.010.
[25] Carpinteri A, Cornetti P, Sapora A. Brittle failures at rounded V-notches: a finite fracture mechanics approach. Int J Fract 2011;172:1–8. https://doi.org/10.1007/s10704-011-9640-8.
[26] Sapora A, Cornetti P, Carpinteri A. V-notched elements under mode II loading conditions. Struct Eng Mech 2014;49:499–508.
[27] Campagnolo A, Berto F, Leguillon D. Fracture assessment of sharp V-notched components under Mode II loading: a comparison among some recent criteria. Theor Appl Fract Mech 2016;85:217–26. https://doi.org/10.1016/j.tafmec.2016.02.001.
[28] Sapora A, Cornetti P, Carpinteri A. A Finite Fracture Mechanics approach to V-notched elements subjected to mixed-mode loading. Eng Fract Mech 2013;97:216–26. https://doi.org/10.1016/j.engfracmech.2012.11.006.
[29] Yosibash Z, Priel E, Leguillon D. A failure criterion for brittle elastic materials under mixed-mode loading. Int J Fract 2006;141:291–312.
[30] Priel E, Yosibash Z, Leguillon D. Failure initiation at a blunt V-notch tip under mixed mode loading. Int J Fract 2008;149:143–73.
[31] Doitrand A, Cornetti P, Sapora A, Estevez R. Experimental and theoretical characterization of mixed mode brittle failure from square holes. Int J Fract 2021;228:33–43. https://doi.org/10.1007/s10704-020-00512-9.
[32] Sapora A, Cornetti P, Campagnolo A, Meneghetti G. Fatigue limit: crack and notch sensitivity by Finite Fracture Mechanics. Theor Appl Fract Mech 2020;105:102407. https://doi.org/10.1016/j.tafmec.2019.102407.
[33] Sapora A, Cornetti P, Campagnolo A, Meneghetti G. Mode I fatigue limit of notched structures: a deeper insight into Finite Fracture Mechanics. Int J Fract 2021;227:1–13. https://doi.org/10.1007/s10704-020-00488-6.
[34] Campagnolo A, Sapora A. A FFM analysis on mode III static and fatigue crack initiation from sharp V-notches. Eng Fract Mech 2021;258:108063.
[35] Wang D, Zhang H, Gong B, Deng C. Residual stress effects on fatigue behaviour of welded T-joint: a finite fracture mechanics approach. Mater Des 2016;91:211–7. https://doi.org/10.1016/j.matdes.2015.11.106.
[36] Ferrian F, Chao Correas A, Cornetti P, Sapora A. Size effects on spheroidal voids by Finite Fracture Mechanics and application to corrosion pits. Fatigue Fract Eng Mater Struct n.d.;n/a. doi:10.1111/ffe.13902.
[37] Shen X, Zeng D, Lu L. Investigating the effect of notch size on critical distance and fatigue limit by coupling the theory of critical distance and finite fracture mechanics. Theor Appl Fract Mech 2022;122:103566. https://doi.org/10.1016/j.tafmec.2022.103566.
[38] Liu Y, Deng C, Gong B. Discussion on equivalence of the theory of critical distances and the coupled stress and energy criterion for fatigue limit prediction of notched specimens. Int J Fatigue 2020;131:105326. https://doi.org/10.1016/j.ijfatigue.2019.105326.
[39] Zhu S-P, He J-C, Liao D, Wang Q, Liu Y. The effect of notch size on critical distance and fatigue life predictions. Mater Des 2020;196:109095. https://doi.org/10.1016/j.matdes.2020.109095.
[40] He J-C, Zhu S-P, Liao D, Niu X-P, Gao J-W, Huang H-Z. Combined TCD and HSV approach for probabilistic assessment of notch fatigue considering size effect. Eng Fail Anal 2021;120:105093. https://doi.org/10.1016/j.engfailanal.2020.105093.
[41] Ciavarella M, D'Antuono P, Demelio GP. Generalized definition of "crack-like" notches to finite life and SN curve transition from "crack-like" to "blunt notch" behavior. Eng Fract Mech 2017;179:154–64. https://doi.org/10.1016/j.engfracmech.2017.04.048.
[42] Basquin OH. The exponential law of endurance tests. Proc Am Soc Test Mater 1910;10:625–30.
[43] Carpinteri A, Paggi M. A unified interpretation of the power laws in fatigue and the analytical correlations between cyclic properties of engineering materials. Int J Fatigue 2009;31:1524–31. https://doi.org/10.1016/j.ijfatigue.2009.04.014.
[44] Castillo E, Fernández-Canteli A, Siegele D. Obtaining S-N curves from crack growth curves: an alternative to self-similarity. Int J Fract 2014;187:159–72. https://doi.org/10.1007/s10704-014-9928-6.
[45] Sanaei N, Fatemi A. Analysis of the effect of internal defects on fatigue performance of additive manufactured metals. Mater Sci Eng A 2020;785:139385. https://doi.org/10.1016/j.msea.2020.139385.
[46] Miarka P, Seitl S, Bílek V, Cifuentes H. Assessment of fatigue resistance of concrete: S-N curves to the Paris' law curves. Constr Build Mater 2022;341:127811. https://doi.org/10.1016/j.conbuildmat.2022.127811.
[47] Williams ML. Stress singularities resulting from various boundary conditions in angular corners of plates in extension. J Appl Mech ASME 1952;19:526–8.
[48] Taylor D, Bologna P, Bel KK. Prediction of fatigue failure location on a component using a critical distance method. Int J Fatigue 2000;22:735–42. https://doi.org/10.1016/S0142-1123(00)00062-1.
[49] DuQuesnay DL, Topper TH, Yu MT. The effect of notch radius on the fatigue notch factor and the propagation of short cracks. Mech Eng Publ Behav Short Fatigue Cracks 1986:323–35.
[50] Mirzaei AM, Ayatollahi MR, Bahrami B, Berto F. A new unified asymptotic stress field solution for blunt and sharp notches subjected to mixed mode loading. Int J Mech Sci 2021;193:106176. https://doi.org/10.1016/j.ijmecsci.2020.106176.
[51] Mirzaei AM, Ayatollahi MR, Bahrami B, Berto F. Elastic stress analysis of blunt V-notches under mixed mode loading by considering higher order terms. Appl Math Model 2020;78:665–84. https://doi.org/10.1016/j.apm.2019.09.049.
[52] Ranjan R, de Oliveira Miranda AC, Hui Guo S, Walbridge S, Gerlich A. Fatigue analysis of friction stir welded butt joints under bending and tension load. Eng Fract Mech 2019;206:34–45. https://doi.org/10.1016/j.engfracmech.2018.11.041.
[53] Nakajima M, Tokaji K, Itoga H, Shimizu T. Effect of loading condition on very high cycle fatigue behavior in a high strength steel. Int J Fatigue 2010;32:475–80. https://doi.org/10.1016/j.ijfatigue.2009.09.003.
[54] Berge S. On the effect of plate thickness in fatigue of welds. Eng Fract Mech 1985;21:423–35. https://doi.org/10.1016/0013-7944(85)90030-X.
[55] Guo W, Wang CH, Rose LRF. The influence of cross-sectional thickness on fatigue crack growth. Fatigue Fract Eng Mater Struct 1999;22:437–44. https://doi.org/10.1046/j.1460-2695.1999.00176.x.
[56] Kim J-K, Shim D-S. The variation in fatigue crack growth due to the thickness effect. Int J Fatigue 2000;22:611–8. https://doi.org/10.1016/S0142-1123(00)00032-3.
[57] Ezeh OH, Susmel L. Fatigue strength of additively manufactured polylactide (PLA): effect of raster angle and non-zero mean stresses. Int J Fatigue 2019;126:319–26. https://doi.org/10.1016/j.ijfatigue.2019.05.014.
[58] Solberg K, Berto F. Notch-defect interaction in additively manufactured Inconel 718. Int J Fatigue 2019;122:35–45. https://doi.org/10.1016/j.ijfatigue.2018.12.021.